

Evaluation of selectivity and sensitivity of gallium nitride nanosensor for grabbing metal/metalloid ions (Na^+ , K^+ , Sn^{2+} , Pb^{2+} , Al^{3+}) from water: materials modelling approach towards environmental treatment

Fatemeh Mollaamin

Department of Biomedical Engineering, Faculty of Engineering and Architecture, Kastamonu University, Kastamonu, Turkey

Received November 11, 2024

The goal of this research is selecting metal/metalloid ions of (Na^+ , K^+ , Sn^{2+} , Pb^{2+} , Al^{3+}) from water due to nanomaterial-based gallium nitride nanocage (Ga–N). Ga–N was modeled in the presence of metal/metalloid cations (Na^+ , K^+ , Sn^{2+} , Pb^{2+} , Al^{3+}). Moreover, the results of chemical shielding calculations exhibited remarkable fluctuations in the metal elements Na^+ , K^+ , Sn^{2+} , Pb^{2+} , Al^{3+} due to the capture of Ga–N in the periodic framework of H_2O molecules. This research work confirms the selectivity of metal ion capture by Ga–N nanodetector as: $\text{K}^+ > \text{Na}^+ >> \text{Sn}^{2+} \approx \text{Pb}^{2+} > \text{Al}^{3+}$. Finally, it has been shown that for a given number of N-donor sites in the Ga–N nanosensor, the stabilities of monovalent (M^+), divalent (M^{2+}) and trivalent (M^{3+}) cation complexes are $\text{K}^+ \leftrightarrow \text{Ga–N} > \text{Na}^+ \leftrightarrow \text{Ga–N} >> \text{Sn}^{2+} \leftrightarrow \text{Ga–N} \approx \text{Pb}^{2+} \leftrightarrow \text{Ga–N} > \text{Al}^{3+} \leftrightarrow \text{Ga–N}$.

Keywords: Metal/lloid ion selection; water purification, Ga–N; nanomaterials application.

Оцінка селективності та чутливості наносенсора з нітриду галію для захоплення іонів металів/металоїдів (Na^+ , K^+ , Sn^{2+} , Pb^{2+} , Al^{3+}) із води: підхід до моделювання матеріалів щодо поводження з навколошнім середовищем.

Fatemeh Mollaamin

Метою даного дослідження є виділення з води іонів металів/металоїдів Na^+ , K^+ , Sn^{2+} , Pb^{2+} , Al^{3+} за допомогою наноклітки нітриду галію (Ga–N) на основі наноматеріалу. Ga–N моделювали в присутності катіонів металів/металоїдів (Na^+ , K^+ , Sn^{2+} , Pb^{2+} , Al^{3+}). Крім того, результати розрахунків хімічного екранування показали значні флюктуації через металеві елементи Na^+ , K^+ , Sn^{2+} , Pb^{2+} , Al^{3+} внаслідок захоплення Ga–N у періодичній сітці молекул H_2O . Ця дослідницька робота підтверджує селективність захоплення іонів металу Ga–N нанодетектором як: $\text{K}^+ > \text{Na}^+ >> \text{Sn}^{2+} \approx \text{Pb}^{2+} > \text{Al}^{3+}$. Нарешті, було показано, що для заданої кількості N-донорних сайтів у Ga–N наносенсорі стабільність одновалентних (M^+), дновалентних (M^{2+}) і тривалентних (M^{3+}) катіонних комплексів $\text{K}^+ \leftrightarrow \text{Ga–N} > \text{Na}^+ \leftrightarrow \text{Ga–N} >> \text{Sn}^{2+} \leftrightarrow \text{Ga–N} \approx \text{Pb}^{2+} \leftrightarrow \text{Ga–N} > \text{Al}^{3+} \leftrightarrow \text{Ga–N}$.

1. Introduction

The chemical characteristics of different elements encountering H_2O molecules in the surface are influenced by geochemical mixture of

atmosphere, soil combination, climate change, and the environmental moods [1–7]. Recently, environmental pollutions produced by hazardous organic materials and toxic metal/metalloid elements with their longevity have become

a fatal barrier [8–15]. For example, Pb is a heavy metal that is found in large quantities in the environment. The development of the life-style and associated production volumes has increased the cost of lead emissions and caused a clear increase in its impurities [16, 17].

Rybarczyk and his co-workers demonstrated the effects of experiments on the synchronic elimination of Al (III), Cu (II), and Zn (II) from dilute aqueous solutions using ion and flash flotation methods. The presented data demonstrate physicochemical processes dependent on metal salts in aqueous solutions [21]. In addition, tin (Sn) is a grey and white metal and appears in the oxidation states of Sn^{2+} and Sn^{4+} cations. Recently, Rathinam et al. have prepared the structurally isomeric rhodamine 6G-based amino derivatives for detecting Sn^{2+} cations [22].

The compressive strength of the Ga–N nanomaterial is quite low, and hence, it is forecasted to enhance the containment of pollutions and overcome the fragile sorption, rapid compression, and secondary contamination in the repair technique. Thus, the goal of this article is to isolate the ions of Na^+ , K^+ , Sn^{2+} , Pb^{2+} , Al^{3+} from the periodic cell of H_2O molecules.

2. Theoretical Insights, applied materials and methods

Material details

The purpose of this research is to take away alkali and alkaline earth metals ions containing Na^+ , K^+ , Sn^{2+} , Pb^{2+} , Al^{3+} from H_2O medium using Ga–N nanomaterial (Fig.1) [23].

The GJF file of the geometry coordination for the encapsulation of metal cations including Na^+ , K^+ , Sn^{2+} , Pb^{2+} , Al^{3+} in Ga–N water was prepared using GaussView 6.1 [24]. Using the solid model and coordination template, the interval line was placed according to the LANL2DZ level of theory to determine the quantum chemical properties (Fig. 1).

The metal cations were successfully incorporated in the center of Ga–N for the formation of $\text{Na}^+ \leftrightarrow \text{Ga–N}$, $\text{K}^+ \leftrightarrow \text{Ga–N}$, $\text{Sn}^{2+} \leftrightarrow \text{Ga–N}$, $\text{Pb}^{2+} \leftrightarrow \text{Ga–N}$, and $\text{Al}^{3+} \leftrightarrow \text{GaN}$ complexes (Fig.1). Regardless of the type of the metal, the gallium nitride nanocage expanded to accommodate the metal particles. Using mixtures of metal nanoparticles of two different sizes, it was found that the inclusion and the resulting pore size were controlled by the larger size metal particles (Fig.1).

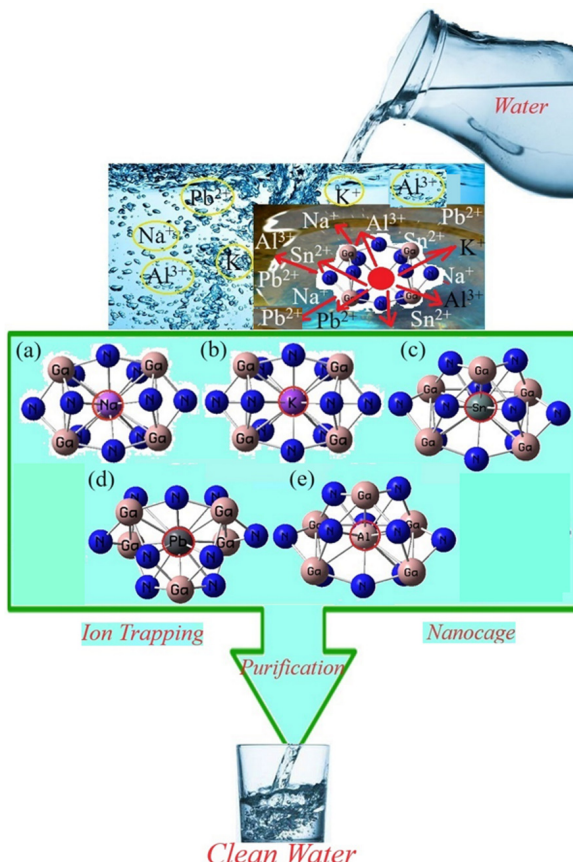


Fig.1. Adsorption of metal/metalloid ions (Na^+ , K^+ , Sn^{2+} , Pb^{2+} , Al^{3+}) from drinking water by Ga–N trough formation of a) $\text{Na}^+ \leftrightarrow \text{Ga–N}$, b) $\text{K}^+ \leftrightarrow \text{Ga–N}$, c) $\text{Sn}^{2+} \leftrightarrow \text{Ga–N}$, d) $\text{Pb}^{2+} \leftrightarrow \text{Ga–N}$, and e) $\text{Al}^{3+} \leftrightarrow \text{GaN}$ complexes for water purification technology

The charge diffusion of $\text{Li}^+ \leftrightarrow \text{Ga–N}$, $\text{Na}^+ \leftrightarrow \text{Ga–N}$, $\text{K}^+ \leftrightarrow \text{Ga–N}$, $\text{Be}^{2+} \leftrightarrow \text{Ga–N}$, $\text{Mg}^{2+} \leftrightarrow \text{Ga–N}$ and $\text{Ca}^{2+} \leftrightarrow \text{Ga–N}$ compounds has been computed according to the Bader charge distribution [25]. The metal ions have been successfully incorporated in the center of Ga–N to form the complexes $\text{Li}^+ \leftrightarrow \text{Ga–N}$, $\text{Na}^+ \leftrightarrow \text{Ga–N}$, $\text{K}^+ \leftrightarrow \text{Ga–N}$, $\text{Be}^{2+} \leftrightarrow \text{Ga–N}$, $\text{Mg}^{2+} \leftrightarrow \text{Ga–N}$, and $\text{Ca}^{2+} \leftrightarrow \text{Ga–N}$ complexes (Fig.1).

Density Functional Theory (DFT) approach

The computational work in this research was performed according to the DFT applying the projector– augmented–wave (PAW) technique [26].

The functions of the Hohenberg-Kohn (HK) theory have rigidly caused the acceptability of electronic density as a fundamental variable for structure/electronic computations. On the other hand, development of the applied DFT methodology became noticeable only after W. Kohn and L.J. Sham published their authorita-

Table 1. The electric potential (E_p /a.u.) and Bader charge (Q/coulomb) through NQR calculation for $\text{Na}^+ \leftrightarrow \text{Ga}-\text{N}$, $\text{K}^+ \leftrightarrow \text{Ga}-\text{N}$, $\text{Sn}^{2+} \leftrightarrow \text{Ga}-\text{N}$, $\text{Pb}^{2+} \leftrightarrow \text{Ga}-\text{N}$, and $\text{Al}^{3+} \leftrightarrow \text{Ga}-\text{N}$ complexes.

$\text{Na}^+ \leftrightarrow \text{Ga}-\text{N}$			$\text{K}^+ \leftrightarrow \text{Ga}-\text{N}$			$\text{Sn}^{2+} \leftrightarrow \text{Ga}-\text{N}$		
Atom	Q	Ep	Atom	Q	Ep	Atom	Q	Ep
Ga1	0.89	-146.60	Ga1	0.87	-146.57	Ga1	0.56	-1.17
N2	-0.48	-18.16	N2	-0.46	-18.17	N2	-0.47	-18.41
N3	-0.51	-18.17	N3	-0.53	-18.18	N3	-0.60	-18.43
Ga4	0.88	-146.60	Ga4	0.83	-146.57	Ga4	0.56	-1.17
Ga5	0.86	-146.62	Ga5	0.87	-146.61	Ga5	0.58	-1.17
Ga6	0.88	-146.63	Ga6	0.90	-146.60	Ga6	0.57	-1.17
N7	-0.46	-18.16	N7	-0.45	-18.16	N7	-0.47	-18.41
N8	-0.51	-18.17	N8	-0.53	-18.17	N8	-0.59	-18.44
N9	-0.49	-18.18	N9	-0.51	-18.19	N9	-0.49	-18.40
N10	-0.50	-18.17	N10	-0.50	-18.18	N10	-0.47	-18.40
N11	-0.47	-18.17	N11	-0.48	-18.18	N11	-0.48	-18.40
N12	-0.54	-18.20	N12	-0.57	-18.20	N12	-0.51	-18.42
Ga13	0.93	-146.61	Ga13	0.86	-146.62	Ga13	0.53	-1.11
N14	-0.45	-18.13	N14	-0.45	-18.13	N14	-0.45	-18.39
N15	-0.44	-18.13	N15	-0.44	-18.12	N15	-0.44	-18.39
Na16	0.42	-34.52	K16	0.60	-74.29	Sn16	2.18	-1.39
$\text{Pb}^{2+} \leftrightarrow \text{Ga}-\text{N}$			$\text{Al}^{3+} \leftrightarrow \text{Ga}-\text{N}$					
Atom	Q	Ep	Atom	Q	Ep			
Ga1	0.60	-1.17	Ga1	0.59	-1.20			
N2	-0.50	-18.42	N2	-0.46	-18.40			
N3	-0.56	-18.44	N3	-0.54	-18.42			
Ga4	0.59	-1.17	Ga4	0.61	-1.20			
Ga5	0.62	-1.17	Ga5	0.63	-1.20			
Ga6	0.59	-1.17	Ga6	0.60	-1.20			
N7	-0.49	-18.41	N7	-0.46	-18.39			
N8	-0.55	-18.44	N8	-0.55	-18.42			
N9	-0.51	-18.42	N9	-0.48	-18.41			
N10	-0.51	-18.43	N10	-0.46	-18.41			
N11	-0.50	-18.42	N11	-0.47	-18.41			
N12	-0.53	-18.44	N12	-0.50	-18.42			
Ga13	0.62	-1.12	Ga13	0.421	-1.18			
N14	-0.43	-18.39	N14	-0.43	-18.38			
N15	-0.44	-18.38	N15	-0.42	-18.38			
Pb16	2.00	-1.37	Al16	1.93	-1.10			

tive series of equations, which are introduced as the Kohn-Sham (KS) equations [27, 28].

In DFT, as it is used for computational chemistry, the hybrid functional Becke 3-parameter Lee-Yang-Parr (B3LYP) [29] appears to offer the greatest contribution. A new hybrid exchange-correlation functional named the Coulomb-Attenuating Method with B3LYP

(CAM-B3LYP) is proposed which combines the hybrid qualities of B3LYP and the long-range correction [30].

In this article, DFT computations were carried out using the Gaussian 16 revision C.01 software [31].

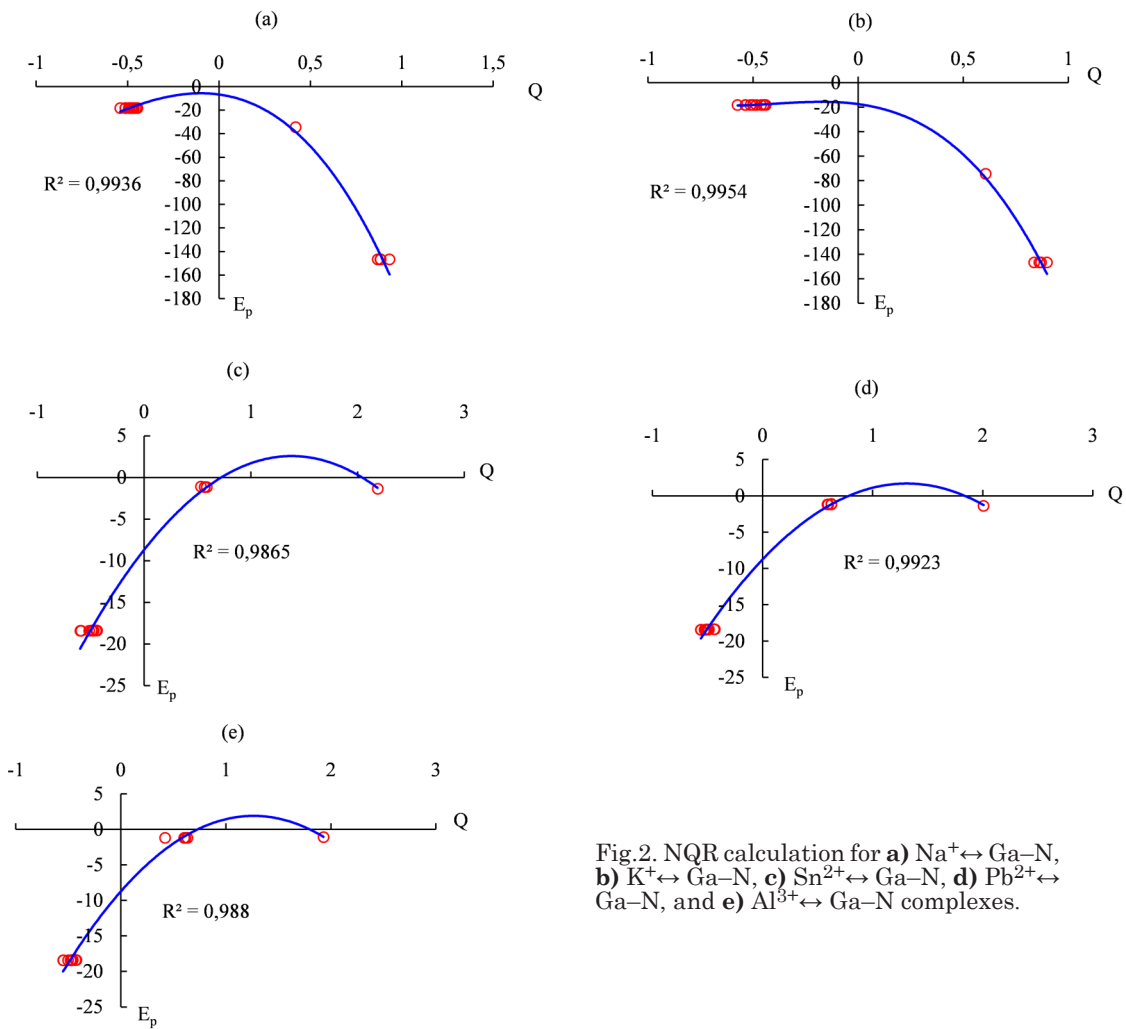


Fig.2. NQR calculation for **a)** $\text{Na}^+ \leftrightarrow \text{Ga}-\text{N}$, **b)** $\text{K}^+ \leftrightarrow \text{Ga}-\text{N}$, **c)** $\text{Sn}^{2+} \leftrightarrow \text{Ga}-\text{N}$, **d)** $\text{Pb}^{2+} \leftrightarrow \text{Ga}-\text{N}$, and **e)** $\text{Al}^{3+} \leftrightarrow \text{Ga}-\text{N}$ complexes.

3. Results and Discussion

Outlook of nuclear quadrupole resonance (NQR)

Since the electric-field gradient when placing the nucleus in metal cations containing Na^+ , K^+ , Sn^{2+} , Pb^{2+} , Al^{3+} is associated with valence electrons wrapped in a certain linkage with close nuclei of $\text{Ga}-\text{N}$ through capturing of metal ions, the NQR [32–35] frequency at which the transitions occur is specific for the complexes (Na^+ , K^+ , Sn^{2+} , Pb^{2+} , Al^{3+}) $\leftrightarrow \text{Ga}-\text{N}$ (Table1).

In addition, the NQR electric potential was constructed for some selected cations Na^+ , K^+ , Sn^{2+} , Pb^{2+} and Al^{3+} in the $\text{Ga}-\text{N}$ which was measured by CAM-B3LYP accompanying the basis sets of EPR-3 and LANL2DZ (Fig. 2a–f).

The Na^+ and K^+ ions in $\text{Na}^+ \leftrightarrow \text{Ga}-\text{N}$ (Fig.2a) and $\text{K}^+ \leftrightarrow \text{Ga}-\text{N}$ complexes (Fig.2b), respectively, have shown approximately the same

behavior with the ratio coefficients of $R^2_{\text{Na}^+} = 0.9954$ and $R^2_{\text{K}^+} = 0.9954$. Furthermore, Sn^{2+} in $\text{Sn}^{2+} \leftrightarrow \text{Ga}-\text{N}$ (Fig.2c), Pb^{2+} in $\text{Pb}^{2+} \leftrightarrow \text{Ga}-\text{N}$ (Fig.2d), Al^{3+} in $\text{Al}^{3+} \leftrightarrow \text{Ga}-\text{N}$ (Fig.2e), respectively, with the ratio coefficients of $R^2_{\text{Sn}^{2+}} = 0.9865$ and $R^2_{\text{Pb}^{2+}} = 0.9923$, $R^2_{\text{Al}^{3+}} = 0.988$, $R^2_{\text{As}^{3+}} = 0.9724$. Since potassium and sodium have electric potential of -74.29 and -34.5186 a.u., respectively, a different fluctuation of charge versus electric potential compared to tin, lead, aluminum, and arsenic were observed (Table1).

NMR spectra Analysis

From the density functional theory (DFT) calculations, it has been achieved the chemical shielding (σ_{aniso}) tensors in the principal axes system to evaluate the isotropic chemical-shielding (σ_{iso}) and anisotropic chemical-shielding (CSA) [36]:

Table 2. Chemical shielding tensors for selected atoms of $\text{Na}^+ \leftrightarrow \text{Ga-N}$, $\text{K}^+ \leftrightarrow \text{Ga-N}$, $\text{Sn}^{2+} \leftrightarrow \text{Ga-N}$, $\text{Pb}^{2+} \leftrightarrow \text{Ga-N}$, and $\text{Al}^{3+} \leftrightarrow \text{Ga-N}$ complexes.

$\text{Na}^+ \leftrightarrow \text{Ga-N}$			$\text{K}^+ \leftrightarrow \text{Ga-N}$			$\text{Sn}^{2+} \leftrightarrow \text{Ga-N}$		
Atom	σ_{iso}	σ_{aniso}	Atom	σ_{iso}	σ_{aniso}	Atom	σ_{iso}	σ_{aniso}
Ga1	176.04	3288.77	Ga1	176.04	3288.77	Ga1	12.10	24.78
N2	146.20	962.64	N2	146.20	962.64	N2	261.54	346.72
N3	559.40	1683.75	N3	559.40	1683.75	N3	218.46	709.28
Ga4	313.19	3636.45	Ga4	313.19	3636.45	Ga4	12.68	19.69
Ga5	664.68	3206.29	Ga5	664.68	3206.29	Ga5	9.94	21.20
Ga6	426.04	2698.25	Ga6	426.04	2698.25	Ga6	13.24	22.75
N7	81.15	707.77	N7	81.15	707.77	N7	194.01	248.04
N8	317.19	1085.00	N8	317.19	1085.00	N8	69.70	648.16
N9	190.49	825.49	N9	190.49	825.49	N9	224.79	351.84
N10	212.97	1100.88	N10	212.97	1100.88	N10	179.19	285.87
N11	183.17	944.69	N11	183.17	944.69	N11	313.78	600.52
N12	41.68	684.33	N12	41.68	684.33	N12	74.47	269.49
Ga13	48.80	1547.56	Ga13	48.80	1547.56	Ga13	14.30	16.71
N14	307.12	507.19	N14	307.12	507.19	N14	342.98	1224.06
N15	339.25	700.60	N15	339.25	700.60	N15	350.77	810.58
Na16	489.74	66.83	K16	489.74	66.83	Sn16	26.47	9.07
$\text{Pb}^{2+} \leftrightarrow \text{Ga-N}$			$\text{Al}^{3+} \leftrightarrow \text{Ga-N}$					
Atom	σ_{iso}	σ_{aniso}	Atom	σ_{iso}	σ_{aniso}			
Ga1	4.60	14.01	Ga1	4.80	20.95			
N2	271.95	537.40	N2	22.61	589.30			
N3	133.15	687.91	N3	665.58	1248.28			
Ga4	9.77	15.74	Ga4	3.59	17.74			
Ga5	4.14	14.66	Ga5	0.98	20.64			
Ga6	9.23	19.27	Ga6	2.57	21.84			
N7	327.68	845.91	N7	168.38	1113.53			
N8	75.74	751.77	N8	552.85	1103.16			
N9	140.10	405.99	N9	178.93	515.87			
N10	238.89	205.71	N10	199.65	483.37			
N11	191.91	577.68	N11	115.46	597.37			
N12	62.87	244.31	N12	93.82	471.38			
Ga13	8.39	9.71	Ga13	6.27	7.16			
N14	358.53	636.87	N14	100.02	330.21			
N15	486.57	857.69	N15	64.09	642.44			
Pb16	24.20	4.52	Al16	16.71	10.27			

$$\sigma_{\text{iso}} = (\sigma_{11} + \sigma_{22} + \sigma_{33}) / 3 \quad (1)$$

$$\sigma_{\text{aniso}} = \sigma_{33} - (\sigma_{22} + \sigma_{11}) / 2 \quad (2)$$

$$\begin{aligned} \sigma_{\text{iso}, \text{ONIOM}} = & \sigma_{\text{iso}, \text{high}(QM1)} + \\ & + \sigma_{\text{iso}, \text{medium}(QM2)} + \sigma_{\text{iso}, \text{low}(QM3)} \end{aligned} \quad (3)$$

The NMR data of isotropic (σ_{iso}) and anisotropic shielding tensor (σ_{aniso}) of Na^+ , K^+ , Sn^{2+} , Pb^{2+} , Al^{3+} captured on the in the Ga-N to form $\text{Na}^+ \leftrightarrow \text{Ga-N}$, $\text{K}^+ \leftrightarrow \text{Ga-N}$, $\text{Sn}^{2+} \leftrightarrow \text{Ga-N}$, $\text{Pb}^{2+} \leftrightarrow \text{Ga-N}$, and $\text{Al}^{3+} \leftrightarrow \text{Ga-N}$ complexes have been computed by the Gaussian 16 revision C.01 program package [31] and shown in Table 2.

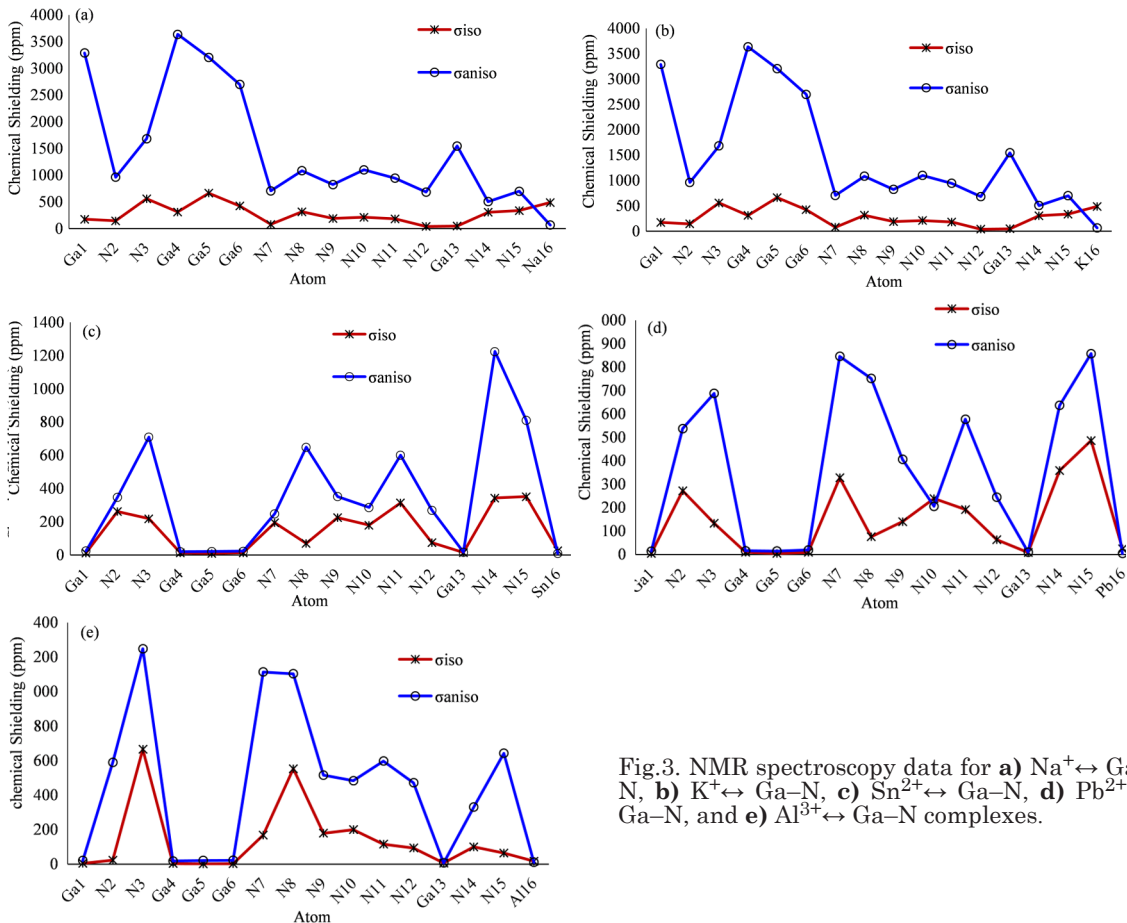


Fig.3. NMR spectroscopy data for a) $\text{Na}^+ \leftrightarrow \text{Ga-N}$, b) $\text{K}^+ \leftrightarrow \text{Ga-N}$, c) $\text{Sn}^{2+} \leftrightarrow \text{Ga-N}$, d) $\text{Pb}^{2+} \leftrightarrow \text{Ga-N}$, and e) $\text{Al}^{3+} \leftrightarrow \text{Ga-N}$ complexes.

The enhancement in the chemical shift anisotropy spans for Ga (4), Ga (5), Ga (6) in $\text{Na}^+ \leftrightarrow \text{Ga-N}$ and $\text{K}^+ \leftrightarrow \text{Ga-N}$ complexes is due to Na^+ , K^+ ions binding to Ga–N (Fig.3a, b). The complexes $\text{Sn}^{2+} \leftrightarrow \text{Ga-N}$ (Fig.3c) and $\text{Pb}^{2+} \leftrightarrow \text{Ga-N}$ (Fig.3d) have shown approximately the similar behavior through the fluctuation of chemical shift anisotropy spans for functionalized atoms N (2), N (3), N (7), N (8), N (9), N (11), N (12), N (14), N (15). Moreover, the $\text{Al}^{3+} \leftrightarrow \text{Ga-N}$ complex (Fig.3e) has shown approximately the similar behavior through the fluctuation of chemical shift anisotropy spans for functionalized atoms of N (2), N (3), N (7), N (8), N (9), N (14), N (15).

In Fig. 3 (a-f), metal ions Na^+ , K^+ , Sn^{2+} , Pb^{2+} , Al^{3+} in $\text{Na}^+ \leftrightarrow \text{Ga-N}$, $\text{K}^+ \leftrightarrow \text{Ga-N}$, $\text{Sn}^{2+} \leftrightarrow \text{Ga-N}$, $\text{Pb}^{2+} \leftrightarrow \text{Ga-N}$ and $\text{Al}^{3+} \leftrightarrow \text{Ga-N}$ complexes illustrate the changes in the chemical shielding in the ion selecting status. As a matter of fact, Fig.3 (a-f) can exhibit the potential of electron accepting during ion capture in the Ga–N as $\text{K}^+ > \text{Na}^+ >> \text{Sn}^{2+} \approx \text{Pb}^{2+} > \text{Al}^{3+}$ that confirms the ability of covalent bond between Ga/N and these ions.

Thermodynamic parameters through IR spectra

The ion \leftrightarrow Ga/N clusters (Fig.1) containing $\text{Na}^+ \leftrightarrow \text{Ga-N}$ (Fig.4a), $\text{K}^+ \leftrightarrow \text{Ga-N}$ (Fig.4b), $\text{Sn}^{2+} \leftrightarrow \text{Ga-N}$ (Fig.4c), $\text{Pb}^{2+} \leftrightarrow \text{Ga-N}$ (Fig.4d), and $\text{Al}^{3+} \leftrightarrow \text{Ga-N}$ (Fig. 4e) has been optimized due to IR spectroscopy data.

Fig.4 (a) shows the frequency range of 100–1150 cm $^{-1}$ for $\text{Na}^+ \leftrightarrow \text{Ga-N}$ with sharp spectral peaks around 281.61, 360.46, 891.95 cm $^{-1}$. Fig.4 (b) shows the changes of frequency of 100–1400 cm $^{-1}$ for $\text{K}^+ \leftrightarrow \text{Ga-N}$ with two strong spectral peaks about 511.8 and 1257.49 cm $^{-1}$. Moreover, Fig.4 (c) shows the frequency range between 200–1200 cm $^{-1}$ for $\text{Sn}^{2+} \leftrightarrow \text{Ga-N}$ with sharp peaks around 254.94, 406.60, 458.02, 593.13, 869.27, 919.83, 995.17, and 1030.76 cm $^{-1}$. Fig.4d shows the frequency range of 200–1200 cm $^{-1}$ for $\text{Pb}^{2+} \leftrightarrow \text{Ga-N}$ with strong spectral peaks about 400.93, 570.63, 861.70, and 1011.39 cm $^{-1}$. Furthermore, the frequency range between 100–1200 cm $^{-1}$ for $\text{Al}^{3+} \leftrightarrow \text{Ga-N}$ with sharp peaks around 134.04, 433.33, 538.19, 669.13, 1103.08 cm $^{-1}$ has been observed (Fig.4e).

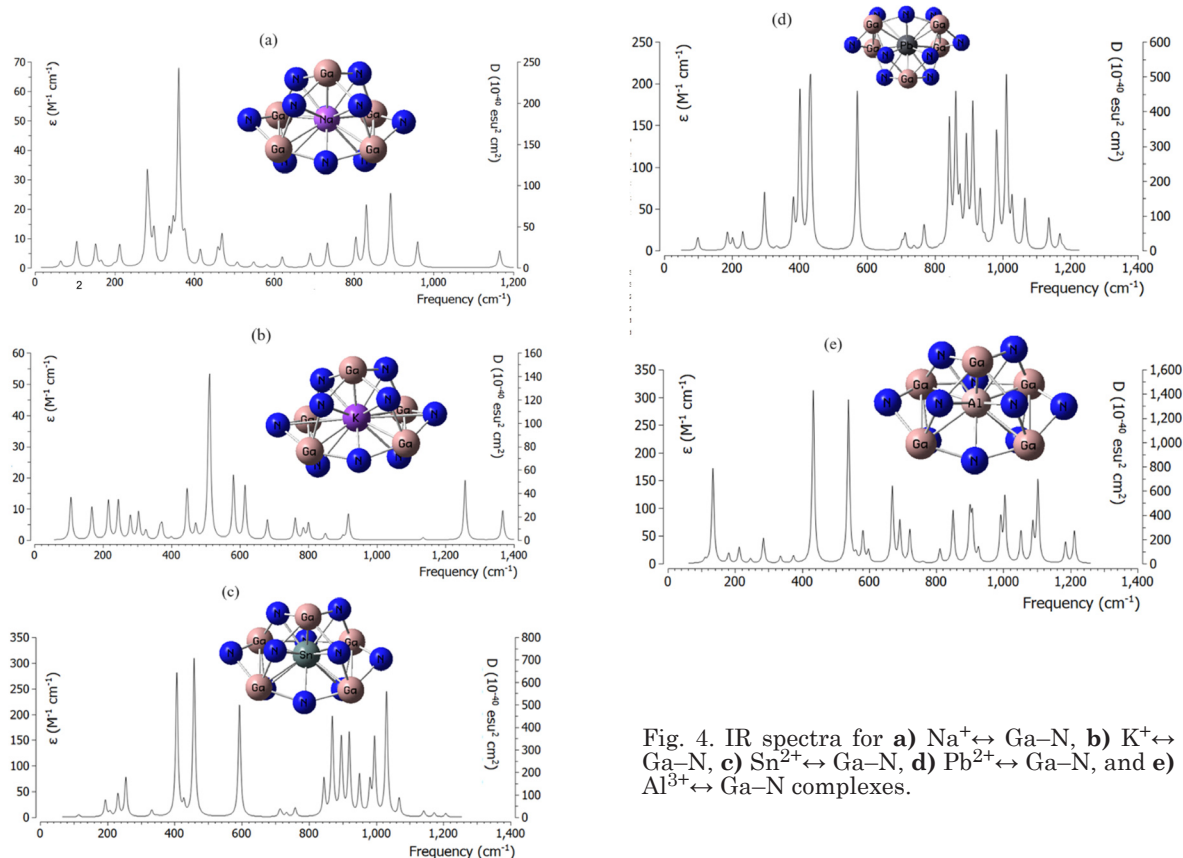


Fig. 4. IR spectra for **a)** $\text{Na}^+\leftrightarrow\text{Ga}-\text{N}$, **b)** $\text{K}^+\leftrightarrow\text{Ga}-\text{N}$, **c)** $\text{Sn}^{2+}\leftrightarrow\text{Ga}-\text{N}$, **d)** $\text{Pb}^{2+}\leftrightarrow\text{Ga}-\text{N}$, and **e)** $\text{Al}^{3+}\leftrightarrow\text{Ga}-\text{N}$ complexes.

In addition, thermodynamic parameters showed that Ga–N, owing to selecting ions of Na^+ , K^+ , Sn^{2+} , Pb^{2+} , Al^{3+} , may be more powerful detector for sensing and taking away ions from water medium (Table 3).

Thermodynamic parameters of complexes of monovalent (M^+), divalent (M^{2+}) and trivalent (M^{3+}) cations with Ga–N have been obtained by the DFT method. The stabilities of M^+ , M^{2+} and M^{3+} in the complexes as $\text{K}^+\leftrightarrow\text{Ga}-\text{N} > \text{Na}^+\leftrightarrow\text{Ga}-\text{N} >> \text{Sn}^{2+}\leftrightarrow\text{Ga}-\text{N} \approx \text{Pb}^{2+}\leftrightarrow\text{Ga}-\text{N} > \text{Al}^{3+}\leftrightarrow\text{Ga}-\text{N}$ are represented in Table 3.

The encapsulation process of metal cations (Na^+ , K^+ , Sn^{2+} , Pb^{2+} , Al^{3+}) in Ga–N is confirmed by $\Delta G_{\text{ads}}^{\circ}$:

Table 3. Thermodynamic characteristics of $\text{Na}^+\leftrightarrow\text{Ga}-\text{N}$, $\text{K}^+\leftrightarrow\text{Ga}-\text{N}$, $\text{Sn}^{2+}\leftrightarrow\text{Ga}-\text{N}$, $\text{Pb}^{2+}\leftrightarrow\text{Ga}-\text{N}$, and $\text{Al}^{3+}\leftrightarrow\text{Ga}-\text{N}$ complexes

Compound	$\Delta E_{\text{o}}\times 10^{-4}$ (kcal/mol)	$\Delta H_{\text{o}}\times 10^{-4}$ (kcal/mol)	$\Delta G_{\text{o}}\times 10^{-4}$ (kcal/mol)	S_{o} (cal/K.mol)	Dipole moment (Debye)
$\text{Na}^+\leftrightarrow\text{Ga}-\text{N}$	-640.72	-640.72	-640.72	110.52	0.31
$\text{K}^+\leftrightarrow\text{Ga}-\text{N}$	-667.87	-667.87	-667.87	99.92	0.53
$\text{Sn}^{2+}\leftrightarrow\text{Ga}-\text{N}$	-350.69	-350.69	-350.72	98.83	1.00
$\text{Pb}^{2+}\leftrightarrow\text{Ga}-\text{N}$	-350.64	-350.64	-350.67	99.45	0.56
$\text{Al}^{3+}\leftrightarrow\text{Ga}-\text{N}$	-350.16	-350.16	-350.19	99.28	0.48

4. Conclusion

Ga–N can effectively select metal/metalloid ions from water medium. Ion selection wrapping a gallium Ga–N nano detector is applied to sweep a series of ions from water medium based on electrostatic interactions between these ions and the Ga–N nanosensor.

Thermodynamic and electromagnetic specifications of metal/metalloid selected by Ga–N nanosensor have been studied by the DFT method. The sensitivity of these ions by Ga–N nanosensor can be represented as: $K^+ > Na^+ >> Sn^{2+} \approx Pb^{2+} > Al^{3+}$. So, it has been concluded that for a given number of N-donor sites in Ga–N, the stability of M^+ are higher than M^{2+} and M^{3+} complexes as $K^+ \leftrightarrow Ga-N > Na^+ \leftrightarrow Ga-N >> Sn^{2+} \leftrightarrow Ga-N \approx Pb^{2+} \leftrightarrow Ga-N > Al^{3+} \leftrightarrow Ga-N$. Furthermore, it is suggested that metal/metalloid-selecting can be applied to ameliorate the optoelectronic specifications of Ga–N which can be employed to generate photoelectric instruments.

Acknowledgment: In successfully completing this paper and its research, the authors are grateful to Kastamonu University.

References

- L. Lajoie, A.-S. Fabiano-Tixier, F. Chemat, *Pharmaceuticals*, **15**, 1507 (2022). <https://doi.org/10.3390/ph15121507>
- M. Wang; Z. Wang, J. Zhang, J. Zhan, C. Wu, W. Yu, W. Fan, J. Tang, Q. Zhang, J. Zhang, *ACS Sustain. Chem. Eng.*, **10**, 10369 (2022). <https://doi.org/10.1021/acssuschemeng.2c03138>
- C. Micheau, A. Schneider, L. Girard, P. Bauduin, *Colloid Surf. A*, **470**, 52 (2015).
- R. Ghosh, A. Sahu, S. Pushpavanam, *J. Hazard. Mater.*, **367**, 589 (2019).
- K. Matsuoka, H. Miura, S. Karima, C. Taketaka, S. Ouno, Y. Moroi, *J. Mol. Liq.*, **263**, 89 (2018).
- G. Lindblom, B. Lindman, G.J.T. Tiddy, *J. Am. Chem. Soc.* **100**, 2299 (1978).
- I.D. Leigh, M.P. McDonald, R.M. Wood, G.J.T. Tiddy, M.H. Trevethan, *J. Chem. Soc. Faraday Trans. 1*, **77**, 2867 (1981).
- N. Schwierz, D. Horinek, R.R. Netz, *Langmuir*, **26**, 7370 (2010).
- M.H. Ropers, G. Czichocki, G. Brezesinski, *J. Phys. Chem. B*, **107**, 5281 (2003).
- L. Lajoie, A.-S. Fabiano-Tixier, F. Chemat, *Pharmaceuticals*, **15**, 1507 (2022). <https://doi.org/10.3390/ph15121507>
- E. Sadatshojaei, D.A. Wood, Water, the Most Accessible Eco-Friendly Solvent, and Extrac-
- tion and Separation Agent. In Green Sustainable Process for Chemical and Environmental Engineering and Science; Elsevier: Amsterdam, The Netherlands, 2021; pp. 283–292. <https://doi.org/10.1016/B978-0-12-821884-6.00012-7>.
- Y. Cheng, F. Xue, S. Yu, S. Du, Y. Yang, *Molecules*, **26**, 4004 (2021). <https://doi.org/10.3390/molecules26134004>
- M. Wang, Z. Wang, J. Zhang, J. Zhan, C. Wu, W. Yu, W. Fan, J. Tang, Q. Zhang, J. Zhang, *ACS Sustain. Chem. Eng.*, **10**, 10369 (2022). <https://doi.org/10.1021/acssuschemeng.2c03138>
- Akira Hiratsuka, Yoshiro Yasuda, *Journal of Water Resource and Protection*, **13**(1), 44-73, (2021). <https://doi.org/10.4236/jwarp.2021.131004>.
- D. A. Gidlow, “Lead toxicity,” *Occupational Medicine*, **65**, no. 5, 348 (2015).
- T. Vincent, P. Krys, C. Jouannin, A.-C. Gaumont, I. Dez, and E. Guibal, *Journal of Organometallic Chemistry*, **723**, 90 (2013).
- J. Czulak, C. Jouannin, T. Vincent, I. Dez, A.-C. Gaumont, and E. Guibal, *Separation Science and Technology*, **47**, no. 14–15, 2166 (2012).
- R. Singh, N. Gautam, A. Mishra, R. Gupta, *Indian Journal of Pharmacology*, **43**, no. 3, 246 (2011).
- S. Zhang, H. Gao, J. Li et al., *Journal of Hazardous Materials*, **321**, 92 (2017).
- Richa Jain. Recent advances of magnetite nanoparticles to remove arsenic from water. *RSC Adv.* 2022 **12**(50): 32197–32209. <https://doi.org/10.1039/d2ra05832d>.
- P. Rybarczyk, B. Kawalec-Pietrenko *Processes.*; **9**(2), 301 (2021). <https://doi.org/10.3390/pr9020301>.
- B. Rathinam, V. Murugesan, B.-T. Liu, *Chemosensors*, **10**, 69 (2022). <https://doi.org/10.3390/chemosensors10020069>.
- R.S. Roy, A. Mondal, & P.K. Nandi, *J. Mol. Model.*, **23**, 93 (2017). <https://doi.org/10.1007/s00894-017-3273-4>
- R. Dennington, T. A. Keith, J.M. Millam, GaussView, Version 6.06.16, Semichem Inc., Shawnee Mission, KS, 2016.
- G. Henkelman, A. Arnaldsson, and H. Jónsson, *Computational Materials Science*, **36**(3), 354 (2006).
- P.E. Blöchl, *Phys. Rev. B*, **50**, 17953 (1994).
- P. Hohenberg, W. Kohn, *Phys. Rev. B*, **136**, B864-B871 (1964).
- Kohn, W., Sham, L. J. Self-Consistent Equations Including Exchange and Correlation Effects. *Phys. Rev.*, 1965, 140, A1133- A1138.
- C. Lee, W. Yang, R.G. Parr, *Phys Rev B*, **37**, 785 (1988).

30. Takeshi Yanai, David P. Tew, Nicholas C. Handy, *Chemical Physics Letters.* **393**(1–3), 51, (2004). <https://doi.org/10.1016/j.cplett.2004.06.011>
31. M. J. Frisch, G. W. Trucks, H. B. Schlegel, G. E. Scuseria, M. A. Robb,; et al. Gaussian 16, Revision C.01, Gaussian, Inc., Wallingford CT, 2016.
32. J. A. S. Smith, *Journal of Chemical Education.* **48**, 39, (1971).
33. K Appendix: Nuclear quadrupole resonance, by Allen N. Garroway, Naval Research Laboratory.
- In Jacqueline MacDonald, J. R. Lockwood: Alternatives for Landmine Detection. Report MR-1608, Rand Corporation, 2003.
34. O. Kh. Poleshchuk, E.L. Kalinna, J. N. Latoinska, J. Koput, *Journal of Molecular Structure (Theochem)* 547 (2001) 233 – 243.
35. A. Young, Hugh, Roger D. Freedman, *Sears and Zemansky's University Physics with Modern Physics* (13th ed.). Boston: Addison-Wesley. p. 754 (2012).